Published in final edited form as:
Small. 2008 March ; 4(3): 372–379. doi:10.1002/smll.200700784.

In Vivo MRI Detection of Gliomas by Chlorotoxin-Conjugated Superparamagnetic Nanoprobes

Conroy Sun, **Omid Veiseh**, **Jonathan Gunn**, and **Chen Fang**
Department of Materials Science & Engineering, University of Washington, Seattle, WA 98195, USA

Stacey Hansen
Clinical Research Division, Fred Hutchinson Cancer Research Center, Seattle, WA 98109, USA

Donghoon Lee
Department of Radiology, University of Washington, Seattle, WA 98195, USA

Raymond Sze
Diagnostic Imaging & Radiology, Children's National Medical Center, Washington DC, 20010, USA

Richard G. Ellenbogen
Department of Neurological Surgery, University of Washington, Seattle, WA 98195, USA

Jim Olson*
Clinical Research Division, Fred Hutchinson Cancer Research Center, Seattle, WA 98109, USA

Miqin Zhang*
Department of Materials Science & Engineering, University of Washington, Seattle, WA 98195, USA

Abstract

Converging advances in the development of nanoparticle-based imaging probes and improved understanding of the molecular biology of brain tumors offer the potential to provide physicians with new tools in the diagnosis and treatment of these deadly diseases. However, the effectiveness of promising nanoparticle technologies is currently limited by insufficient accumulation of these contrast agents within tumors. Here we present a biocompatible nanoprobe composed of a poly (ethylene glycol) (PEG) coated iron oxide nanoparticle that is capable of specifically targeting glioma tumors via the surface-bound targeting peptide, chlorotoxin (CTX). The preferential accumulation of the nanoprobe within gliomas and subsequent magnetic resonance imaging (MRI) contrast enhancement were demonstrated *in vitro* in 9L cells and *in vivo* in tumors of a xenograft mouse model. TEM imaging revealed that the nanoprobes were internalized into the cytoplasm of 9L cells and histological analysis of selected tissues indicated no acute toxic effects of these nanoprobes. High-targeting specificity and benign biological response establish this nanoprobe as a potential platform to aid in the diagnosis and treatment of gliomas and other tumors of the neuroectodermal origin.

Keywords

nanoparticles; nanotechnology; biomaterials; cancer; imaging

[*] Miqin Zhang, Ph.D., Department of Materials Science & Engineering, 302L Roberts Hall, University of Washington, Seattle, WA 98195-2120, Phone: (206) 616 9356, Fax: (206) 543 3100, E-mail: E-mail: mzhang@u.washington.edu; and Jim Olson, M.D., Ph.D., Fred Hutchinson Cancer Research Center, Mailstop D4-100, 1100 Fairview Ave. N., Seattle, WA 98109, E-mail: E-mail: jimmyo@u.washington.edu.

1. Introduction

Despite recent advances in brain cancer therapy, such as improved surgical techniques and multimodal adjuvant therapy, the prognosis remains poor for patients diagnosed with malignant gliomas, the most common primary tumor of the central nervous system (CNS).[1] In its most aggressive form, glioblastoma multiforme, patients experience a mean survival of less than 1 year.[2] Insufficient treatment is largely due to challenges in eliminating tumor cells, which often infiltrate normal tissue or lie adjacent to delicate anatomical structures of the brain. Complete surgical resection of neoplastic tissue has corresponded to improved survival rates,[3,4] but patient recovery is still hindered by an inability to accurately locate tumor cells and distinguish them from healthy neurological tissue. For lower grade, less aggressive gliomas, surgical resection is the mainstay of treatment. Radical resection of low grade gliomas often depends on the surgeon's ability to navigate through brain and separate the neoplasm from the normal brain, which may represent a challenge. Improved demarcation of tumor from normal tissue during surgery will likely lead to improved, more radical resections, fewer neurological deficits and thus, safer surgery and improved patient outcomes. Currently, gadolinium chelate contrast-enhanced magnetic resonance imaging (MRI) is the primary method for detection and pre-operative localization of brain tumors due to its high spatial resolution and non-invasive nature. Unfortunately, this powerful imaging modality is still limited in its inability to accurately delineate tumor boundaries and quantify tumor volumes as a result of surrounding edema and diffusion of contrast agents from the tumor site.

Superparamagnetic iron oxide nanoparticles have been evaluated as MRI contrast agents to improve the differentiation of neoplastic from normal brain tissue.[5,6] In comparison to conventional gadolinium chelates, nanoparticle-based contrast agents offer prolonged delineation of tumor margins due to enhanced cellular internalization and slower clearance from the tumor site.[5,7] Currently, several formulations of iron oxide particles have been approved by the FDA for clinical applications such as bowel (i.e., Lumiren and Gastromark) and liver/spleen imaging (i.e., Endorem and Feridex IV)[8] due to their effective reduction of proton relaxation time. However, these current systems rely on passive targeting, including uptake by cells of the reticuloendothelial system (RES) surrounding the tumor site[5,6], rather than direct cancer cell labeling. The next generation of tumor specific contrast agents, known as molecularly-targeted imaging agents, is expected to offer significantly improved tumor detection and localization by exploiting the unique molecular signature of cancer cells.[9,10] Recent advances in the understanding of the underlying biological mechanisms of gliomas coupled with improvements in nanoparticle technology provide exciting new opportunities for diagnosis and treatment of this disease which has seen little improvement in survivability over the past three decades.[11,12]

In this study, we demonstrate an MRI nanoprobe that targets gliomas (in principle, any tumors expressing membrane-bound matrix metalloproteinase-2) with high-level specificity both *in vitro* and *in vivo*. The nanoprobe is composed of an iron oxide core coated with polyethylene glycol (PEG) and conjugated with the targeting agent, chlorotoxin (CTX). CTX, a 36 amino acid peptide, has recently become the focus of intense research due to its high selectivity for, and binding affinity to, gliomas as well as other tumors of the neuroectodermal origin.[13,14] We previously showed that CTX specifically binds to glioma, medulloblastoma, prostate cancer, sarcoma, and intestinal cancer.[15] Thus it is possible that CTX-conjugated nanoparticles will be useful for most cancers that express membrane-bound MMP-2. Currently, an iodine-131 linked version of CTX is under Phase II clinical trials for targeted radiation of tumor cells.[16] In our previous work, we have demonstrated the effectivity of *in vitro* targeting of glioma cells using a CTX-conjugated nanoparticle.[17] Here we present an alternative, improved process for the synthesis of CTX-conjugated nanoprobes and demonstrate its ability to specifically target gliomas through both *in vitro* and *in vivo* evaluation.

The tumor specificity of the nanoprobe was evaluated *in vitro* using a 9L gliosarcoma cell line through cellular uptake assays and *in vivo* by MR imaging of athymic (nu/nu) mice bearing xenografts, a widely used and well-established animal model mimicking natural gliomas.[18,19] Nanoparticle internalization by glioma cells was visualized by transmission electron microscopy (TEM) and quantified by measuring the intracellular iron content using a colorimetric assay. The targeted contrast enhancement of tumor cells was demonstrated with both *in vitro* MR phantom imaging and *in vivo* small animal MR imaging. R2 relaxation rates were measured to quantify the degree of contrast enhancement. Additionally, histological analysis was performed on tissues from clearance organs, where significant nanoprobe accumulation is expected, to investigate for signs of acute toxicity.

2. Results and Discussion

Amine functionalized PEG-coated nanoparticles (NP-PEG-NH_2) were prepared by a process described in our previous work.[20] Nanoparticles synthesized by this method exhibited a core size of 10-15 nm by TEM and were stable in phosphate buffered saline (PBS), without flocculating, for several months.[21] Biocompatible PEG serves as a coating to reduce protein adsorption and non-specific macrophage uptake, ultimately prolonging serum half-life *in vivo*.[22,23] Well-established for its non-fouling properties, PEG is FDA-approved and employed in a wide variety of biomedical applications.[24] Here PEG also serves as a linking agent providing terminal functional groups for the conjugation of ligands, such as CTX and potential therapeutic agents with iron oxide nanoparticles. The number of reactive amine functional groups available for conjugation of ligands was determined to be ~30 per nanoparticle by quantification of pyridine-2-thione following reaction with N-succinimidyl 3-(2-pyridyldithio)-propionate (SPDP).[25] The conjugation of the targeting agent CTX, a recombinant peptide originally purified from the venom of the *Leiurus quinquestriatus* scorpion, was performed through a three-step reaction illustrated in Figure 1. Initially, a free sulfhydryl group was grafted to CTX through modification with 2-Iminothiolane-HCl (Traut's Reagent; Figure 1a), as opposed to the heterobifunctional linker, N-succinimidyl-S-acetylthioacetate (SATA) which was previously utilized at this stage. NP-PEG-NH_2 was then reacted with succinimidyl iodoacetate (SIA) to yield sulfhydryl reactive nanoparticles (NP-PEG-SIA; Figure 1b). Upon combination of the thiol-modified CTX with the NP-PEG-SIA (Figure 1c), stable thioether linkages were formed between the nanoparticle and the peptide. The resulting NP-PEG-CTX nanoprobe was purified by GPC chromatography and stored in PBS for subsequent use. The improved synthetic procedure eliminates the SATA deprotection and purification processes and produces higher yield of products, substantially reducing overall processing time and potential contamination.

Nanoparticle surface modification and CTX conjugation were confirmed by Fourier transform infrared spectroscopy (FTIR). IR spectra of (a) bare iron oxide nanoparticles, (b) NP-PEG-NH_2, and (c) NP-PEG-CTX are shown in Figure 2. The spectrum for the bare nanoparticles (a) exhibits peaks characteristic of iron oxide, most notably that of -OH found on the oxide surface at 3400 cm^{-1}. Following surface modification with the amine-terminal PEG silane (b), methylene peaks at 2916 and 2860 cm^{-1} were observed. Successful PEG attachment is further confirmed by the carbonyl bands at 1642 and 1546 cm^{-1} which correspond to the amide bonds within the structure of the bifunctional PEG silane.[20] The peak at 1105 cm^{-1} corresponding to the Si-O bond confirms the bonding between the silane and the nanoparticle. Following CTX conjugation (c), the methyl symmetric/asymmetric stretch located at 2960 cm^{-1} corresponding to the alanine residues of the CTX is observed. The broad peak at 1631 cm^{-1} indicates that both primary and secondary amines in residues such as lysine and arginine are present. Additionally, the peaks at 1422 cm^{-1} and 1380 cm^{-1} indicate carbonyl and C-C stretching, respectively, found in the peptide.

The targeting specificity of NP-PEG-CTX for glioma cells was assessed by the intracellular uptake of this nanoprobe in comparison to a non-targeting NP-PEG-SIA control. 9L cells were incubated with the nanoprobes at a concentration range of 0-150 μg Fe/ml for 2 hrs at 37°C. Nanoprobe uptake was quantified by intracellular iron content determined by a colorimetric ferrozine-based assay.[26] Figure 3 displays the intracellular iron content per cell after incubation. Both nanoprobes exhibited concentration dependent uptake that tended to saturate at high particle concentrations. Significantly higher intracellular iron content was observed in cells incubated with the NP-PEG-CTX than those incubated with NP-PEG-SIA at all nanoprobe concentrations indicating the preferential binding of the NP-PEG-CTX targeting probe to 9L cells. An approximate 10-fold increase in preferential uptake was observed at the highest nanoprobe concentration tested (150 μg Fe/mL). The minimal NP-PEG-SIA uptake by 9L cells at the highest nanoprobe concentration, is believed to be attributed to the PEG coating on nanoparticles, which has been shown to facilitate nanoparticle internalization into cancer cells.[22,27]

Localization of nanoprobes in the cells was visualized with TEM (Figure 4) which shows 9L cells incubated with either NP-PEG-SIA (a) or NP-PEG-CTX (b) at a concentration of 100 μg Fe/mL for 1 hr at 37°C prior to fixation for microscopy. Consistent with the nanoparticle uptake assay (Figure 3), no appreciable NP-PEG-SIA nanoparticle accumulation was observed in the 9L cells (Figure 4a). In comparison, NP-PEG-CTX nanoprobes were clearly observed in the cytoplasm of the cells (Figure 4b). The presence of these nanoprobes in the lysozomes indicates the nanoprobes were internalized by the cells after binding to the membrane surface. This result is consistent with the receptor-mediated endocytosis of CTX upon preferential binding to MMP-2.[13] The high-magnification image reveals that the nanoprobes maintain their original morphology and size within the cytoplasm of the cells. The internalization of the nanoprobe suggests their ability to provide persistent MRI contrast enhancement as well as their potential to serve as a carrier for drug delivery.

We then examined the efficacy of CTX-conjugated nanoprobes to target glioma cells and provide contrast enhancement for MRI. MRI phantom experiments were performed using 9L cells exposed to the nanoprobes under the same conditions described above. After cell culture, cells were suspended and encased in an agarose mold at a concentration of 1×10^{-7} cells/mL for MR imaging. A series of MR images were acquired using a conventional spin-echo pulse sequence on a 4.7T spectrometer, with varying echo times (TE) to construct an R2 (1/T2) relaxivity map for each sample. T2-weighted MR images and R2 color maps of samples containing 9L cells incubated with various concentrations of the nanoprobes are shown in Figure 5. Compared to the tumor cells incubated with the non-targeting NP-PEG-SIA (Figure 5a), cells incubated with the NP-PEG-CTX (Figure 5b) displayed a significant negative contrast enhancement (darkening) and higher R2 relaxivity at each of the nanoprobe concentrations tested. The signal enhancement observed in the cells incubated with the targeting nanoprobe is consistent with the uptake results describe above. The R2 relaxivity determined from the slope of the linear fit for cells cultured with the NP-PEG-CTX nanoprobe (5.20 ms/mmol) displayed a ~24-fold higher relaxation rate than that observed for the cells incubated with the non-targeting NP-PEG-SIA (0.22 ms/mmol) further signifying the targeted contrast enhancement of the targeting NP-PEG-CTX.

The efficacy of the nanoprobe to specifically target gliomas and provide MRI contrast enhancement *in vivo* were evaluated with nude mice bearing 9L xenograft tumors. The specificity of the nanoprobes was evaluated by comparing the contrast enhancement of the tumor regions of mice receiving NP-PEG-CTX and those receiving NP-PEG-SIA at the same concentration, as well as comparing the contrast enhancement between tumor and normal tissue regions. Initially, anatomical images were acquired in the coronal and sagittal planes to determine the tumor position along the flank of the animal, as shown in Figures 6a and 6b,

respectively. Axial cross-sectional images were then acquired through the tumor region using multi-spin echo pulse sequences to obtain a series of images over a range of TEs. Each mouse was imaged prior to, and at various time points after, intravenous injection of the nanoprobes at a dosage of 6 mg Fe/kg. R2 relaxivity maps were then generated to quantify contrast enhancement resulting from the accumulation of the nanoprobes. The preferential targeting of the glioma tumor in mice receiving the NP-PEG-CTX (Figure 6d), in comparison to NP-PEG-SIA (Figure 6c), was evident in MR images acquired 3 hrs post-injection. Tumor contrast enhancement in the superimposed R2 change map displays a significantly higher intensity and a more thorough enhancement of the overall tumor in the mouse injected with NP-PEG-CTX than in the mouse receiving the NP-PEG-SIA non-targeting probe. The inhomogeneous distribution of the nanoprobes observed in the tumor is due to heterogeneous nature of this type of tumor which is consistent with other reported studies.[28,29] Slight accumulation of the NP-PEG-SIA in the tumor is believed due to the enhanced permeability and retention (EPR) effect common for nanoparticles[30,31] and nonspecific uptake by glioma cells at the tumor margin.[32,33] This result also suggests that although a non-targeting nanoprobe may accumulate in tumors through the passive uptake by cells, as demonstrated in other nanoparticle systems,[5-7,29,32,33] targeting nanoprobes can significantly increase the particle accumulation and thus the contrast enhancement. Importantly, targeting nanoprobes can differentiate between tumor and muscle cells and thus preferentially accumulate in tumor over normal tissue regions as demonstrated below. This not only enhances the identification of tumor regions for more thorough surgical resection and reduces collateral damage to surrounding healthy tissue, but also allows for potential targeted drug delivery at low-dosage administration reducing toxic side effects.

The accumulation and retention of the targeting nanoprobe in tumor and surrounding normal tissue were evaluated at intervals of 0, 0.3, 2, 12, and 24 hrs post-injection to quantify the nanoprobe accumulation and define the time window when animals can be imaged to achieve the maximum MRI contrast, as well as to gain an understanding of the pharmacokinetics of this nanoprobe. This was done by monitoring the change in R2 in tumor (Figure 7a) and normal (Figure 7b) tissues over time. Nanoprobe accumulation in the tumor increased sharply upon injection of the NP-PEG-CTX nanoprobe and up to a maximum at the 12 hr time point resulting in R2 change of ~16 ms^{-1}. At 24 hrs, the change in R2 for the tumor region dropped to ~10 ms^{-1}. The result indicates that the nanoprobe has a prolonged blood half-life sufficient to reach and accumulate in the target tumor prior to clearance by the liver or spleen and that the best imaging window is 2-25 hrs post-injection. The prolonged retention of the nanoprobe in tumors (in tens of hours) may prove to be particularly valuable in clinical settings. Compared to tumors, adjacent muscle showed only a maximum change of less than 5 ms^{-1} in R2 that occurred also at 12 hr imaging time point, which is significantly less than the R2 change in tumor. These results further support the specificity of these nanoprobes for glioma tumors and correlate well with the results obtained from the *in vitro* assays shown above.

Finally, we performed histological analysis on tissues obtained from various clearance organs (kidney, spleen, and liver), in which nanoprobe accumulation was expected to occur, to investigate for signs of acute toxicity. Tissues were harvested 2 days after injection of the nanoprobes and fixed in 10% formalin, embedded in paraffin, sectioned and stained with hematoxylin and eosin (H&E). Tissue sections (Figure 8) were reviewed by a pathologist with expertise in veterinary pathology for evidence of tissue toxicity. No apparent toxicity was observed in the tissues from the animals receiving the nanoprobes in comparison to mice receiving no injection. Furthermore, mice injected with nanoprobes underwent physical and neurologic evaluations to detect any acute toxicity associated with the administration of the nanoprobes. No differences in eating, drinking, grooming, exploratory behavior, activity, physical features (e.g., coat quality), or neurologic status were observed between the mice injected with nanoprobes and the mice receiving no nanoprobes.

3. Conclusions

Advances in molecular targeting and nanoparticle-based therapeutic and diagnostic platforms are expected to offer tremendous potential toward improving the diagnosis and treatment of tumors. Here we have combined the concepts from these two fields to create a targeting nanoprobe and demonstrated its high-level specificity to target gliomas both *in vitro* and *in vivo* as well as its ability to serve as a MRI contrast enhancement agent. In comparison studies with control nanoprobes, we showed a profound difference between targeting and non-targeting nanoprobes in tumor labeling efficiency, which may be attributed to the ligand-receptor mediated nanoprobe internalization by target cells. Combined with prolonged retention in tumors and no apparent acute toxicity, this nanoprobe may allow for earlier cancer detection, tumor staging, and therapy assessment. With PEG functional groups available on the nanoparticle, this nanoprobe allows for conjugation of other diagnostic and therapeutic agents to develop nanoplatforms for both improved visualization and targeting drug delivery.

4. Experimental Section

Materials

All materials were purchased from Sigma-Aldrich (St. Louis, MO) unless otherwise stated.

Synthesis of nanoprobes

The synthesis of core iron oxide nanoparticles and surface modification with an amine functionalized PEG coating was reported previously.[20,21] Iodoacetate functionalized nanoparticles were prepared by adding 5 mg of succinimidyl iodoacetate (SIA; Molecular Bioscience, Boulder, CO), dissolved in 0.15 mL of dimethyl sulfoxide (DMSO), to a 1.5 mL suspension of NP-PEG-NH_2 (4 mg Fe/mL) in 100 mM sodium bicarbonate (pH 8.5). The solution was protected from light and placed on a shaker for 2 hrs at room temperature. The nanoparticles were then purified by GPC chromatography using Sephacryl S-200 resin (GE Healthcare, Piscataway, NJ) equilibrated with thiolation buffer (deoxygenated PBS, 5mM ethylenediamine tetraacetic acid adjusted to pH 8.00). Concurrently, a sulfhydryl group was attached to the CTX peptide (Alomone Labs Ltd., Jerusalem, Israel) via primary amine modification by treatment with Traut's Reagent (Molecular Bioscience, Boulder, CO). Initially, a 1 mg/mL Traut's Reagent stock solution was prepared in the thiolation buffer. Then 6 μL of this stock solution was added to 1.5 mg of CTX (1 mg/mL dissolved in thiolation buffer) and allowed to react for 1 hr at room temperature. Upon completion of thiolation reaction, the peptide solution was mixed with the iodoacetate functionalized nanoparticles for 1 hr at room temperature. Finally, excess CTX was purified from the nanoprobes by column chromatography using Sephacryl S-200 resin equilibrated with PBS.

Nanoprobe characterization

Surface chemical properties of bare iron oxide nanoparticles, NP-PEG-NH_2 and NP-PEG-CTX nanoprobe were characterized by FTIR. For each sample, 2 mg of dried nanoparticles was mixed with 200 mg of KBr and pressed into a pellet for analysis. FTIR spectra were acquired using a Nicolet 5-DXB FTIR spectrometer (Thermo Scientific, Boston, MA) with a resolution of 4/cm.

In vitro nanoprobe uptake assay

To evaluate the efficacy of NP-PEG-CTX nanoprobes in targeting glioma cells, cellular uptake of the nanoprobe was compared against control nanoprobes (NP-PEG-SIA) by incubation with 9L gliosarcoma cells (ATCC, Manassas, VA). Initially, 9L cells were plated on 12-well plates and cultured in DMEM (Invitrogen, Carlsbad, CA) supplemented with 10% FBS and 1% penicillin/streptomycin at 37°C in a humidified atmosphere with 5% CO_2. Cells were incubated

for 1-2 days until they reached 80% confluence. Cells were then washed twice with PBS and incubated with DMEM containing 0-150 μg Fe/mL nanoprobes for 2 hrs at 37°C. The cells were then washed three times with PBS and lysed with 50 mM NaOH (300 μl). Intracellular iron content was determined by quantifying iron content by the colorimetric ferrozine-based assay and determining cell count by protein quantification [26]. Specifically, 300 μl of the cell lysates were added to 300 μl of 10 mM HCl and 300 μl of an iron release reagent composed of equal volumes of 4.5% (w/v) and 1.4M HCl. Similarly, samples of known iron concentration (0-1.0 μg Fe/ml) were prepared to establish a standard curve. The mixtures were incubated at 60°C for 2 hrs and then allowed to cool to room temperature. 90 μl of a solution containing 6.5 mM ferrozine, 6.5 mM neocuproine, 2.5 M ammonium acetate, and 1 M ascorbic acid dissolved in water, was then added to each sample. The absorbance of each sample was read at 562 nm and fitted against the linear standard curve to determine iron concentration. Cell concentrations for each sample were determined by Coomassie Blue protein quantification assay. 300 μl of the Coomassie Blue reagent were added to 6 μl of each lysed cell sample solution and standard solutions containing 0.5-4.0 million untreated cells per ml. Samples and standards were analyzed at an absorbance of 595 nm. Samples were then fitted to a standard curve (quadratic fit) to determine cell count.

In vitro MRI

Cell samples were prepared by dispersing cells in equal volumes of 1% low melting agarose at 40°C. Samples were then quickly transferred to sample holders and chilled at -20°C until gelation. MR imaging was performed on a 4.7-T magnet (Bruker Medical Systems, Karlsruhe, Germany) with a Varian INOVA console (Varian, Inc., Palo Alto, CA). T2-weighted spin echo multisection pulse sequences with a repetition time (TR) of 2000 ms and echo time (TE) of 60 ms were used. The spatial resolution parameters were set as follows: acquisition matrix of 256 × 128, field of view of 35 × 35 mm, section thickness of 2 mm, and 2 averages.

Xenograft preparation

All mouse studies were conducted in accordance with IACUC approved protocols. Subcutaneous xenografts were established in athymic (nu/nu) mice using a 9L rat gliosarcoma cell line (ATCC). The xenografts were established using 1 million 9L cells suspended in serum free media and matrigel at a 1:1 ratio.

In vivo MRI

Nanoprobes were administered via retro-orbital injections. Mice were anesthetized with 1 to 2.5% isoflurane (Abbott Labs, Abbott Park, IL) before they were placed in the imaging chamber and imaged before injection and at various time points post-injection. A multispin echo multislice imaging sequence was used to determine T2 values in tumor and normal tissues using the following imaging parameters: TR = 4 s, TE = 20, 40, 60, 80 ms, field of view of 40 × 40 mm^2, number of averages of 2, matrix size of 256 × 128, slice thickness of 1 mm, slice gap of 0.1 mm, and 10 slices. Multi-echo multi-slice images were performed on a 4.7 T magnet (Bruker Medical Systems) equipped with Varian INOVA spectrometer (Varian, Inc.). Spin-spin relaxation time T2 maps were generated from the multi-echo images with TEs ranging from 20 to 80 ms.

Animal evaluation & histology

Mice injected with the nanoprobes underwent physical and neurologic evaluations. In addition, histologic analysis of tissues was performed 2 days post-injection. Immediately after each mouse was sacrificed, tissues were removed and fixed in 10% formalin for at least 24 hrs. The formalin fixed sections were then paraffin-embedded, sectioned and stained with hematoxylin

and eosin (H&E) per standard clinical laboratory protocol. Tissue sections were reviewed by a pathologist with expertise in veterinary pathology.

Acknowledgements

This work was supported by NIH/NCI Nanoplatform (R01CA119408), NIH/NCI Unconventional Initiative Program (N01CO37122), and a graduate fellowship awarded under the University of Washington NSF-IGERT Program in Nanotechnology. We would like to acknowledge Forrest M Kievit and Cindy Yuen for their laboratory assistance, Sue E. Knoblaugh for histological review, and the University of Washington Diagnostic Imaging Sciences Center (DISC) for MRI facilities.

References

[1]. CBTRUS, Central Brain Tumor Registry of the United States (CBTRUS). Chicago: 2006.

[2]. Behin A, Hoang-Xuan K, Carpentier AF, Delattre JY. Lancet 2003;361:323–331. [PubMed: 12559880]

[3]. Nazzaro JM, Neuwelt EA. J Neurosurg 1990;73:331–344. [PubMed: 2166779]

[4]. Nitta T, Sato K. Cancer 1995;75:2727–2731. [PubMed: 7743477]

[5]. Enochs WS, Harsh G, Hochberg F, Weissleder R. J Magn Reson Imaging 1999;9:228–232. [PubMed: 10077018]

[6]. Neuwelt EA, Varallyay P, Bago AG, Muldoon LL, Nesbit G, Nixon R. Neuropathol Appl Neurobiol 2004;30:456–471. [PubMed: 15488022]

[7]. Varallyay P, Nesbit G, Muldoon LL, Nixon RR, Delashaw J, Cohen JI, Petrillo A, Rink D, Neuwelt EA. AJNR Am J Neuroradiol 2002;23:510–519. [PubMed: 11950637]

[8]. Wang YX, Hussain SM, Krestin GP. Eur Radiol 2001;11:2319–2331. [PubMed: 11702180]

[9]. Ferrari M. Nature Reviews Cancer 2005;5:161–171.

[10]. Weissleder R. Science 2006;312:1168–1171. [PubMed: 16728630]

[11]. Sathornsumetee S, Reardon DA, Desjardins A, Quinn JA, Vredenburgh JJ, Rich JN. Cancer. 2007

[12]. Nakada M, Nakada S, Demuth T, Tran NL, Hoelzinger DB, Berens ME. Cell Mol Life Sci 2007;64:458–478. [PubMed: 17260089]

[13]. Lyons SA, O'Neal J, Sontheimer H. Glia 2002;39:162–173. [PubMed: 12112367]

[14]. Kachra Z, Beaulieu E, Delbecchi L, Mousseau N, Berthelet F, Moumdjian R, Del Maestro R, Beliveau R. Clin Exp Metastasis 1999;17:555–566. [PubMed: 10845554]

[15]. Veiseh M, Gabikian P, Bahrami SB, Veiseh O, Zhang M, Hackman RC, Ravanpay AC, Stroud MR, Kusuma Y, Hansen SJ, Kwok D, Munoz NM, Sze RW, Grady WM, Greenberg NM, Ellenbogen RG, Olson JM. Cancer Res 2007;67:6882–6888. [PubMed: 17638899]

[16]. Mamelak AN, Jacoby DB. Expert Opin Drug Deliv 2007;4:175–186. [PubMed: 17335414]

[17]. Veiseh O, Sun C, Gunn J, Kohler N, Gabikian P, Lee D, Bhattarai N, Ellenbogen R, Sze R, Hallahan A, Olson J, Zhang M. Nano Lett 2005;5:1003–1008. [PubMed: 15943433]

[18]. Weizsaecker M, Deen DF, Rosenblum ML, Hoshino T, Gutin PH, Barker M. J Neurol 1981;224:183–192. [PubMed: 6162014]

[19]. Barth RF. J Neurooncol 1998;36:91–102. [PubMed: 9525831]

[20]. Kohler N, Fryxell GE, Zhang M. J Am Chem Soc 2004;126:7206–7211. [PubMed: 15186157]

[21]. Sun C, Sze R, Zhang M. J Biomed Mater Res A 2006;78:550–557. [PubMed: 16736484]

[22]. Zhang Y, Kohler N, Zhang M. Biomaterials 2002;23:1553–1561. [PubMed: 11922461]

[23]. Weissleder R, Bogdanov A, Neuwelt EA, Papisov M. Advanced Drug Delivery Reviews 1995;16:321–334.

[24]. Veronese FM, Pasut G. Drug Discov Today 2005;10:1451–1458. [PubMed: 16243265]

[25]. Hogemann D, Josephson L, Weissleder R, Basilion JP. Bioconjug Chem 2000;11:941–946. [PubMed: 11087345]

[26]. Riemer J, Hoepken HH, Czerwinska H, Robinson SR, Dringen R. Anal Biochem 2004;331:370–375. [PubMed: 15265744]

[27]. Zhang Y, Sun C, Kohler N, Zhang M. Biomed Microdevices 2004;6:33–40. [PubMed: 15307442]

[28]. Huh YM, Jun YW, Song HT, Kim S, Choi JS, Lee JH, Yoon S, Kim KS, Shin JS, Suh JS, Cheon J. J Am Chem Soc 2005;127:12387–12391. [PubMed: 16131220]

[29]. Medarova Z, Pham W, Farrar C, Petkova V, Moore A. Nat Med 2007;13:372–377. [PubMed: 17322898]

[30]. Moghimi SM, Hunter AC, Murray JC. Pharmacol Rev 2001;53:283–318. [PubMed: 11356986]

[31]. Maeda H. Adv Enzyme Regul 2001;41:189–207. [PubMed: 11384745]

[32]. Zimmer C, Weissleder R, Poss K, Bogdanova A, Wright SC Jr. Enochs WS. Radiology 1995;197:533–538. [PubMed: 7480707]

[33]. Zimmer C, Wright SC Jr. Engelhardt RT, Johnson GA, Kramm C, Breakefield XO, Weissleder R. Exp Neurol 1997;143:61–69. [PubMed: 9000446]

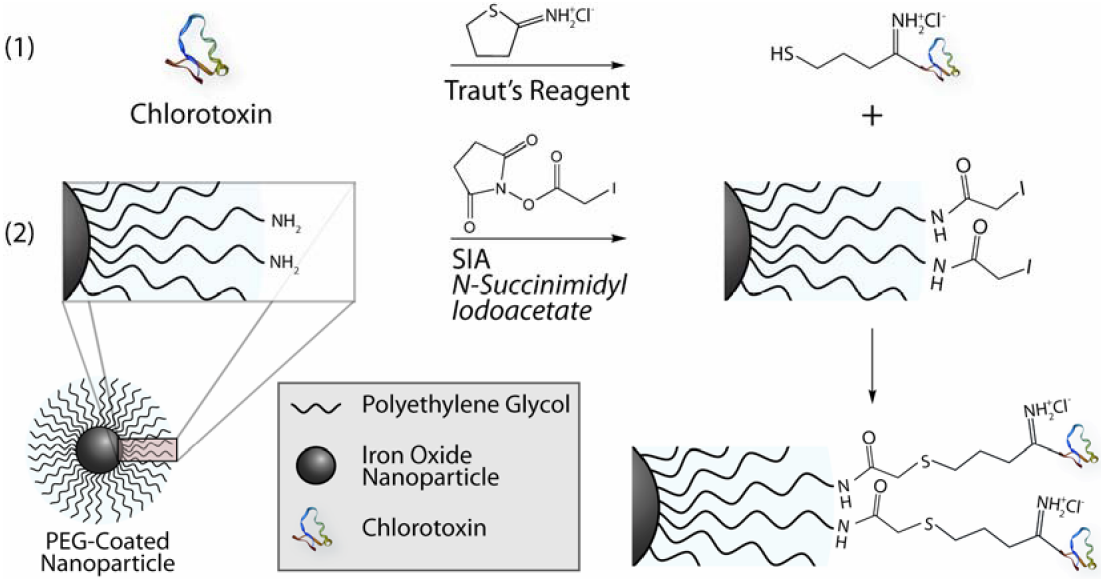

Figure 1.

Illustration of CTX conjugation to PEG-amine coated nanoparticles. Chemical reaction scheme for (a) adding a free sulfhydryl reactive group to CTX via Traut's Reagent, (b) iodoacetate functionalization of NP-PEG-NH_2, and (c) formation of a thioether linkage between the nanoparticle and CTX.

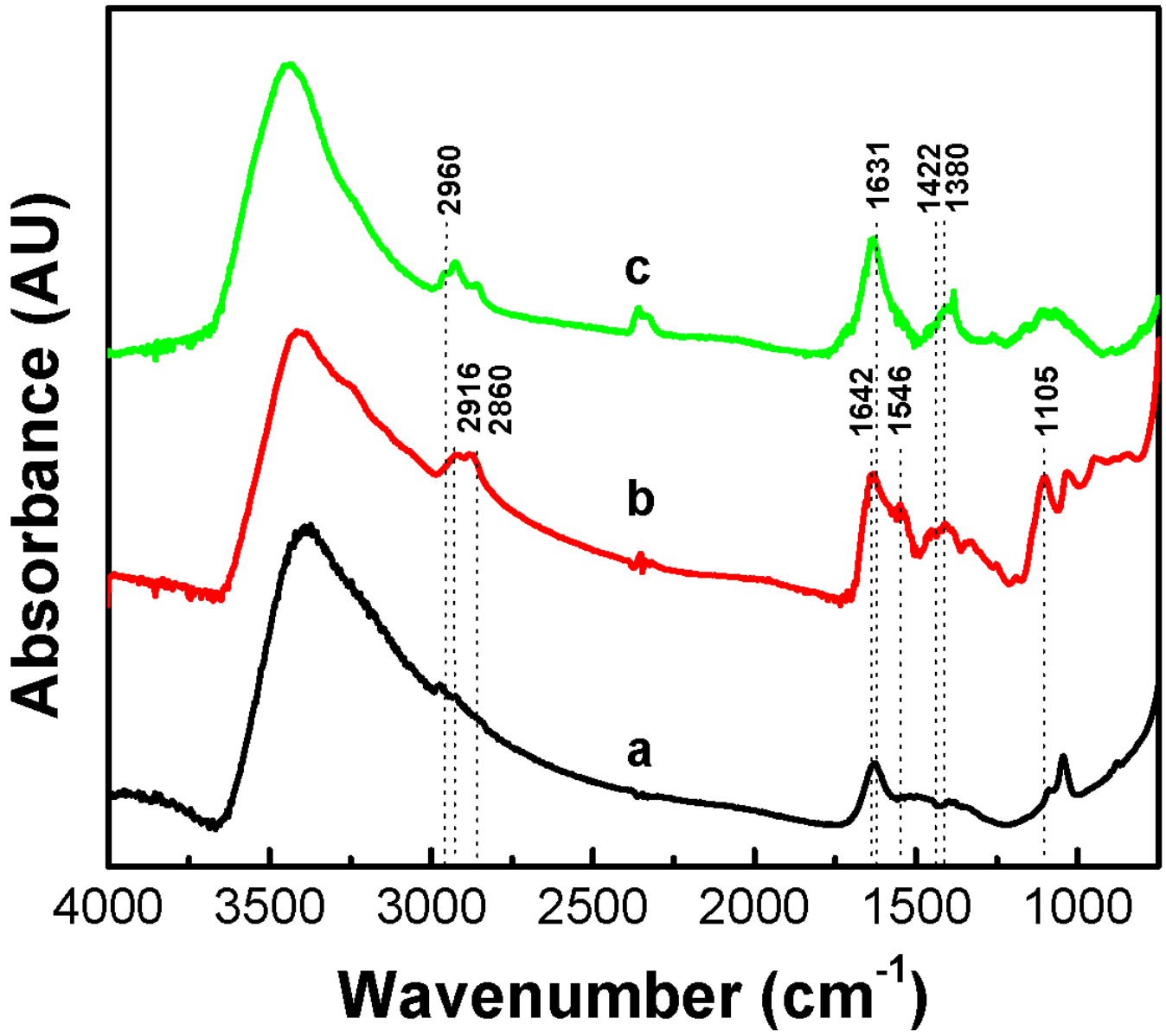

Figure 2.
FTIR spectra of (a) bare nanoparticles, (b) NP-PEG-NH_2, and (c) NP-PEG-CTX.

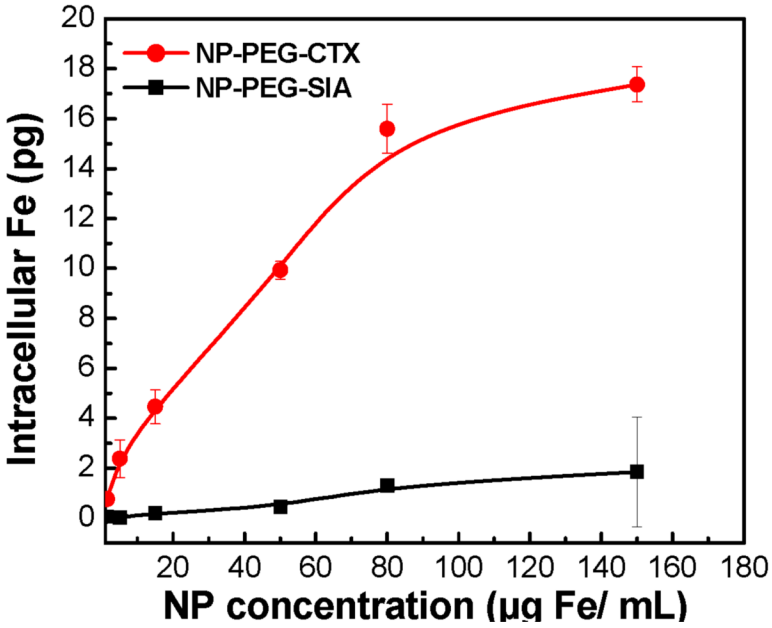

Figure 3.
Uptake of nanoprobes by 9L cells as determined by ferrozine assays.

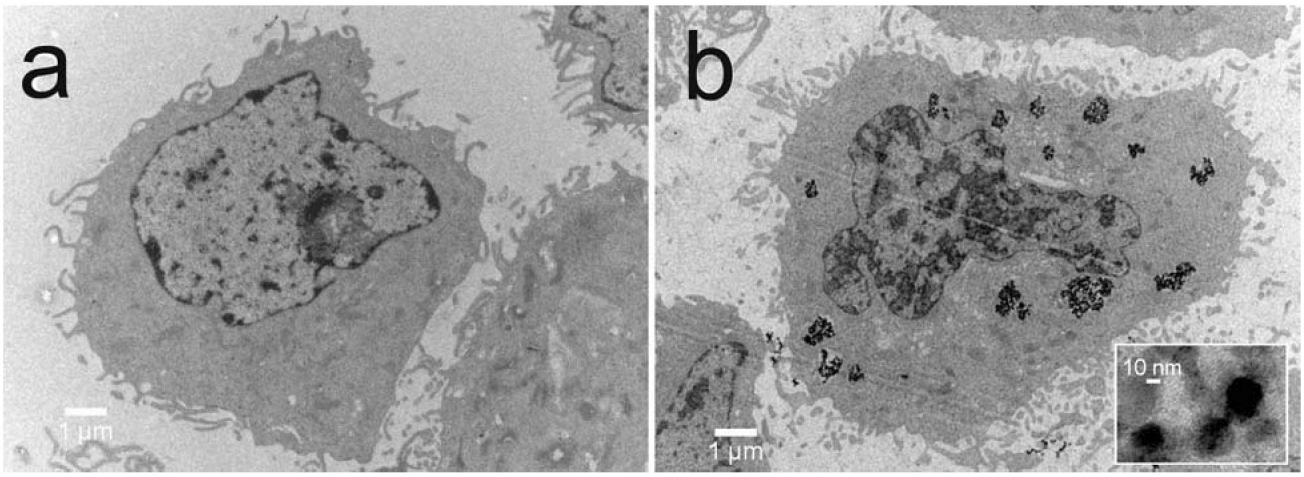

Figure 4.
TEM images of 9L cells incubated with (a) NP-PEG-SIA and (b) NP-PEG-CTX.

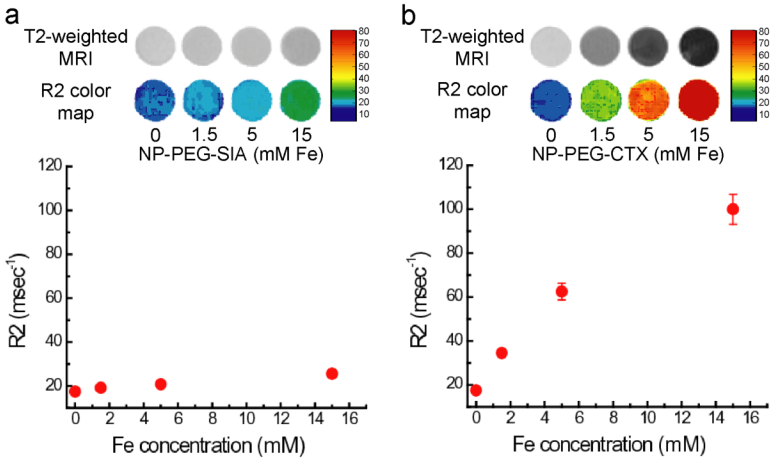

Figure 5.

T2-weighted MR phantom images and corresponding R2 relaxivity maps of 9L cells incubated with (a) NP-PEG-SIA and (b) NP-PEG-CTX. R2 values plotted as a function of incubation concentration display a near linear correlation consistent with the nanoprobe uptake described above.

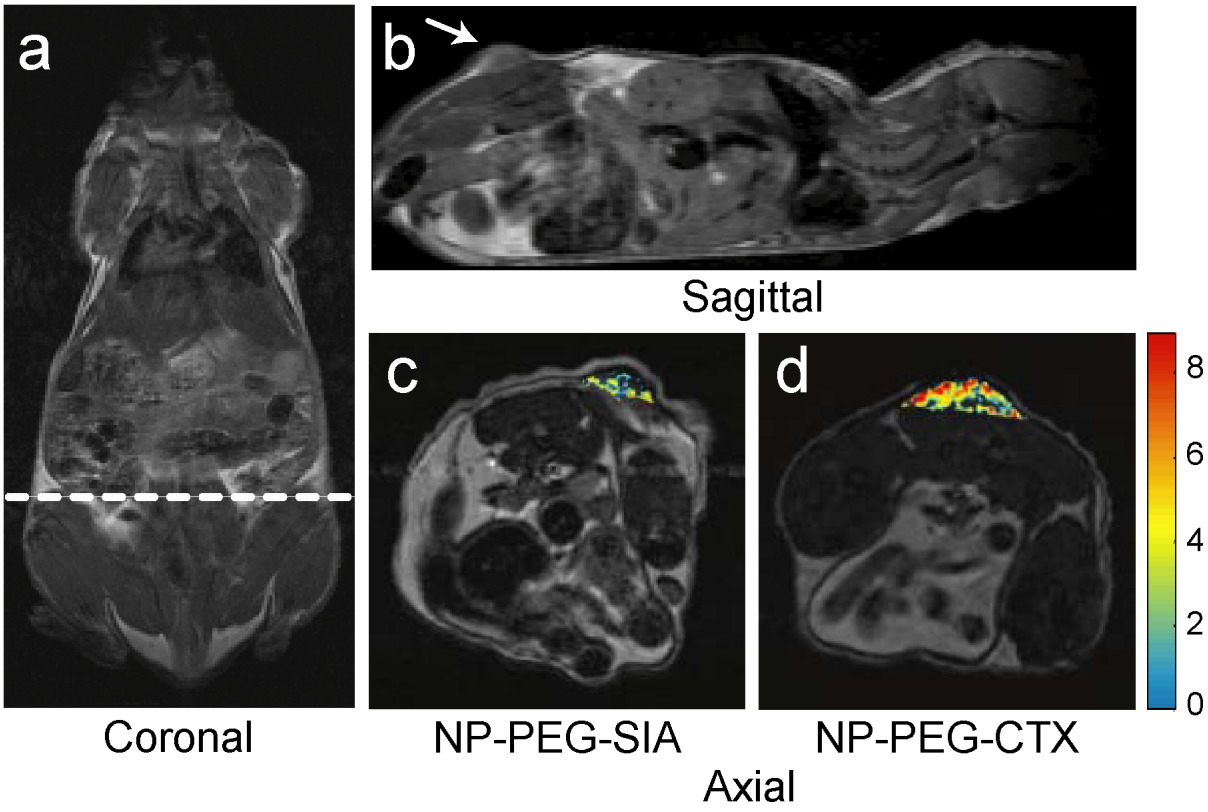

Figure 6.
Representative images from three independent experiments with similar results. MRI anatomical image of a mouse in the (a) coronal plane with the dotted line displaying the approximate location of the axial cross sections displayed in (c) and (d). Anatomical image in the (b) sagittal plane displaying the location of the 9L xenograft tumor. Change in R2 relaxivity values for the tumor regions (superimposed over anatomical MR images) for mouse receiving (c) non-targeting NP-PEG-SIA and (d) NP-PEG-CTX 3 hrs post injection. The white arrow in (b) marks the tumor location.

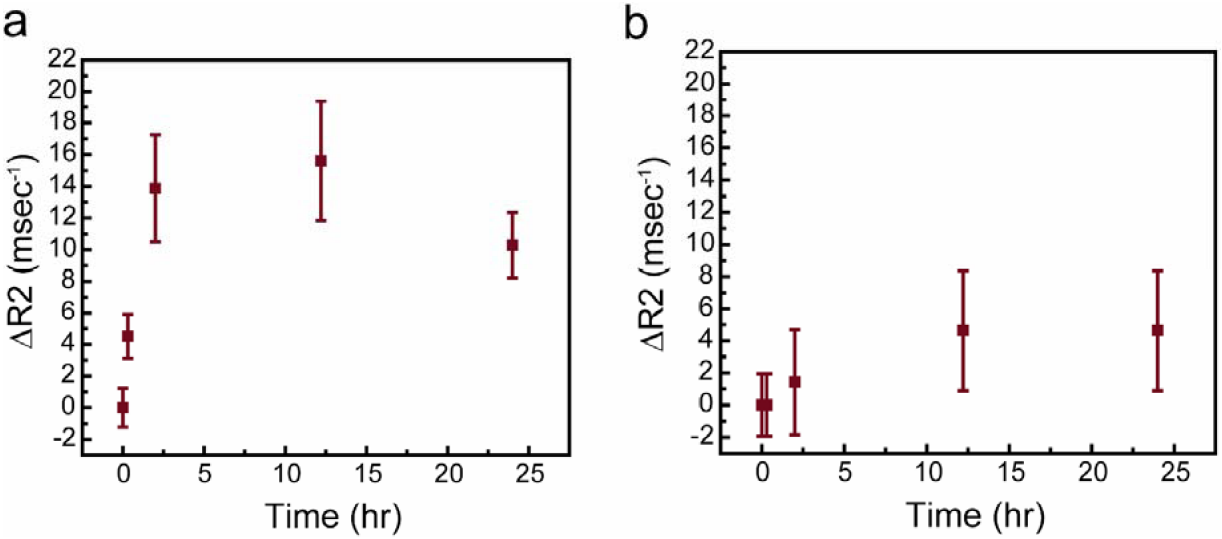

Figure 7.

Change in R2 relaxivity in (a) tumor and (b) normal tissue regions in mice injected with NP-PEG-CTX over a time course of 24 hrs post-injection. Mean values were obtained from three independent experiments with the error bars displaying the standard deviation of the measurements.

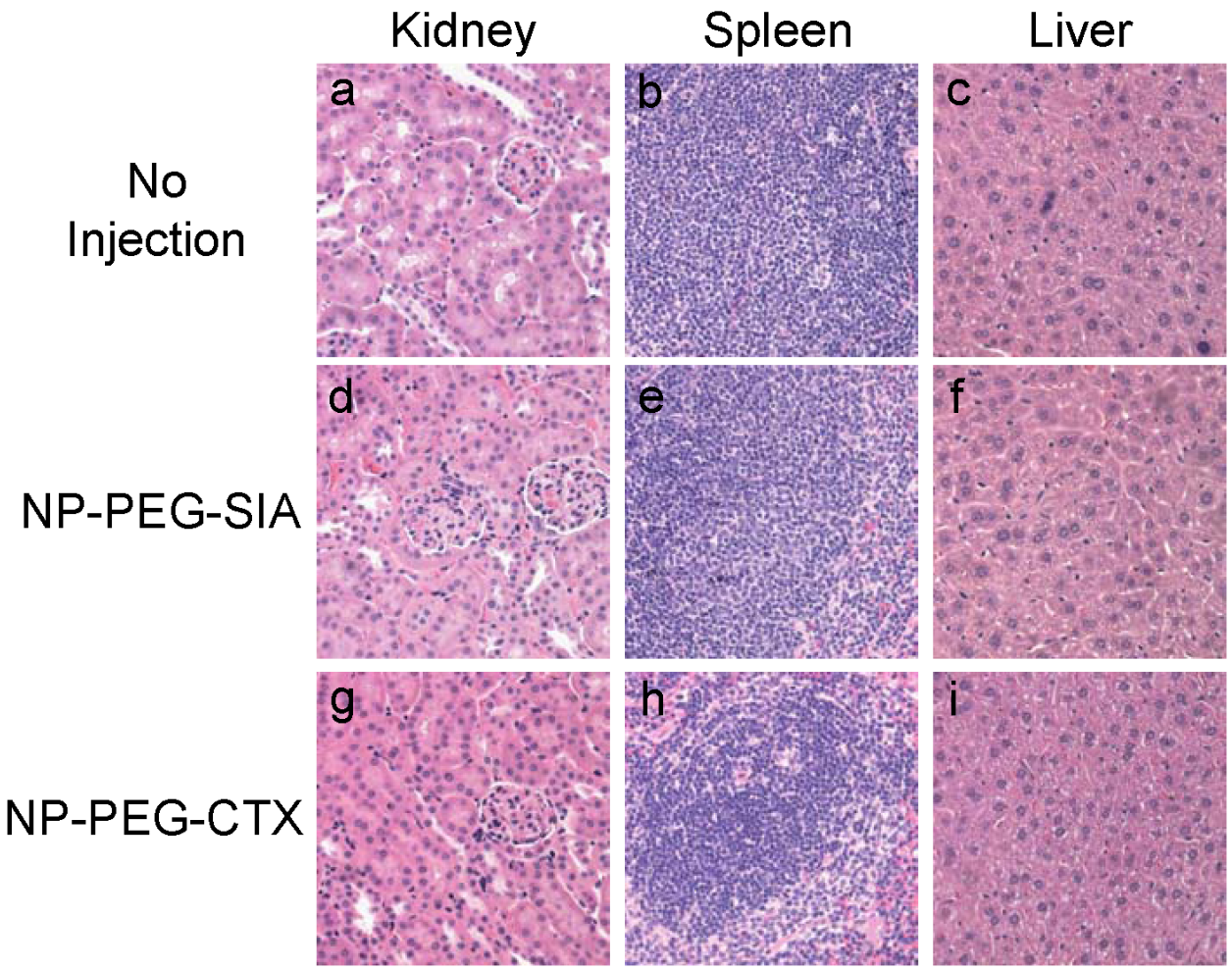

Figure 8.
H &E stained tissue sections from mice receiving no injection (a,b,c) and mice injected with NP-PEG-SIA (d, e, f) or NP-PEG-CTX (g, h, i) 2 days post-injection. Tissues were harvested from kidney, spleen, and liver, respectively.